Continuous Nanoflow-SECM: Voltammetric Characterization and Application to Accurate and Reproducible Imaging of Enzyme-Labeled Protein Microarrays.

ARTICLE *in* ANALYTICAL CHEMISTRY · APRIL 2015

Impact Factor: 5.64 · DOI: 10.1021/acs.analchem.5b00625 · Source: PubMed

4 AUTHORS:

Tianhan Kai

California State University, Los Angeles

6 PUBLICATIONS **3** CITATIONS

SEE PROFILE

Shu Chen

Hunan University of Science and Technology

33 PUBLICATIONS **203** CITATIONS

SEE PROFILE

Estuardo Monterroso

California State University, Los Angeles

2 PUBLICATIONS **1** CITATION

SEE PROFILE

Feimeng Zhou

California State University, Los Angeles

136 PUBLICATIONS **4,807** CITATIONS

SEE PROFILE

analytical chemistry

Article

pubs.acs.org/ac

Continuous Nanoflow-Scanning Electrochemical Microscopy: Voltammetric Characterization and Application for Accurate and Reproducible Imaging of Enzyme-Labeled Protein Microarrays

Tianhan Kai,[#] Shu Chen,[#] Estuardo Monterroso,[†] and Feimeng Zhou*[,†]

[#]College of Chemistry and Chemical Engineering, Central South University, Changsha, Hunan 410083, China

[†]Department of Chemistry and Biochemistry, California State University, Los Angeles, Los Angeles, California 90032, United States

ABSTRACT: The coupling of scanning electrochemical microscopy (SECM) to a continuous nanoflow (CNF) system is accomplished with the use of a microconcentric ring electrode/injector probe. The gold microring electrode encapsulated by a glass sheath is robust and can be beveled and polished. The CNF system, comprising a precision gas displacement pump and a rotary valve, is capable of delivering solution to the center of the SECM probe in the range of 1−150 nL/min. Major advantages of the CNF-SECM imaging mode over the conventional SECM generation/collection (G/C) mode include higher imaging resolution, immunity from interferences by species in the bulk solution or at other sites of the substrate, elimination of the feedback current that could interfere with the G/C data interpretation, and versatility of initiating surface reactions/processes via introducing different reactants into the flowing stream. Parameters such as flow rates, probe/substrate separations, and collection efficiencies are examined and optimized. Higher resolution, reproducibility, and accuracy are demonstrated through the application of CNF-SECM to horseradish peroxidase (HRP)-amplified imaging of protein microarrays. By flowing H_2O_2 and ferrocenemethanol through the injector and detecting the surface-generated ferriceniummethanol, human IgG spots covered with HPR-labeled antihuman IgG can be detected in the range of 13 nM−1.333 μM with a detection limit of 3.0 nM. In addition, consistent images of microarray spots for selective and high-density detection of analytes can be attained.

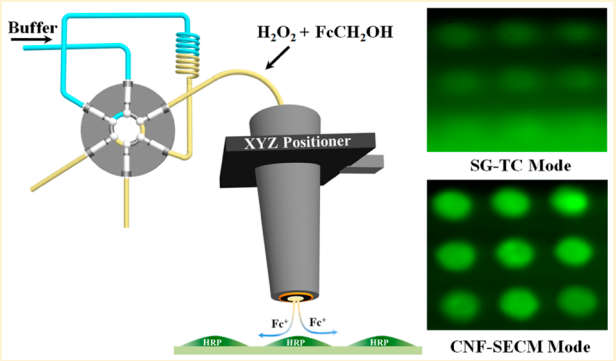

Scanning electrochemical microscopy (SECM)[1,2] has been firmly established as an important scanning probe microscopic (SPM) technique, as reflected by its widespread applications described in various reviews[3−6] and inclusion as a topic in textbooks for undergraduate and graduate students.[7,8] Compared to other SPM techniques such as scanning tunneling microscopy and atomic force microscopy, SECM is a chemical imaging tool that is powerful for studying highly localized chemical reactions and redox properties of surfaces or adsorbates and for inducing redox reactions at the solution/solid interface.[2−6] SECM imaging can be conducted in the feedback mode wherein the probe current is perturbed by a substrate in close proximity.[2,7] The increase and decrease in the probe current, or SECM positive and negative feedback, are dependent on whether the probe-generated redox species can be regenerated at the substrate.

An alternative SECM imaging mode is the generation/collection (G/C) mode, which has two variants. The tip (probe) generation-substrate collection (TG-SC) variant is more suitable for studies of electrode reactions,[9] whereas the substrate generation-tip collection (SG-TC) counterpart is more popular for surface imaging, especially for mapping out reactive sites on a particular surface. We should note that the feedback mode in many cases is not amenable to mapping surface activities or detecting surface-generated species. Unfortunately, the resolution of the SG-TC mode is generally lower, owing to the larger diffusion field of the active site(s) at the surface than that at the smaller probe. This problem exacerbates when there are multiple closely spaced active sites at the sample, as the diffusion layers of such sites continuously propagate in the radial direction and eventually overlap with one another.[7] Samples containing multiple closely spaced active sites include DNA/protein microarrays,[10−14] rows of catalyst candidates,[15,16] immobilized cells of various organisms,[17−21] and materials comprising many reactive spots or centers.[22,23] In biological imaging or sensor development, a common strategy is to use enzyme-tagged antibodies or ligands for either enhanced molecular recognition or amplified signals.[6,24−26] The enzymes used include horseradish peroxidase, glucose oxidase, and alkaline phosphatase.[27−30] For example, the following catalytic cycle has been utilized for SECM imaging of cells, sensors, and microarrays:

Received: February 13, 2015
Accepted: April 1, 2015
Published: April 1, 2015

DOI: 10.1021/acs.analchem.5b00625
Anal. Chem. 2015, 87, 4523−4529

Over immobilized HRP molecules:

$$H_2O_2 + 2H^+ + 2HRP_{red} \rightarrow 2HRP_{ox} + 2H_2O \quad (1)$$

$$FcCH_2OH + HRP_{ox} \rightarrow FcCH_2OH^+ + HRP_{red} \quad (2)$$

At the SECM probe electrode:

$$FcCH_2OH^+ + e^- = FcCH_2OH \quad (3)$$

where HRP_{red} and HRP_{ox} represent the reduced and oxidized forms of horseradish peroxidase (HRP) and $FcCH_2OH$ (ferrocenemethanol) is the SECM mediator. Thus, overlap of diffusion layers will become particularly acute when cells immobilized in high density or multiple spots on a microarray are tagged with enzyme molecules. This is because generation of products at the substrate is accelerated by enzyme molecules. The accelerated reaction results in a more rapid product buildup in the SECM solution and creates a continually increasing background that adversely impacts the SECM detection level and reproducibility. These problems could be somewhat alleviated by spacing out of the active sites, which in practice might not be possible to control during the substrate preparation or will reduce the analysis throughput as in the case of microarrays. Alternatively, one can raster the probe at a higher rate. However, the image quality will be significantly compromised.

We envision that the above-mentioned problems are best circumvented by using a probe capable of simultaneously delivering fresh solution of the enzyme substrate or an SECM mediator to the probe/substrate gap and detecting the substrate-generated species. Among the various capillary flow probes reported in the literature,[31−33] a metal-coated pulled capillary insulated with electrophoretic paint[33,34] could serve these purposes. Bard and co-workers filled their probe with a redox mediator using a microinjector prior to immersing it into an SECM solution.[33] A single injection of the mediator allowed them to image a Pt disk substrate. However, the potential advantages of this probe over the conventional disk-shaped SECM probe have not been attained, as the collection efficiency under the experimental condition is about only 1%.[33] Moreover, the electrode, with a long aspect ratio and a thin layer of electrophoretic paint, is rather fragile for routine imaging. This could be the reason why thus far no analytical utility has been explored. What has also remained unknown is how redox cycling or hindered diffusion inherent in SECM imaging will be impacted by the high mass transfer rate associated with the radial flow.[35−37]

To mitigate these limitations, we recently constructed a robust microring electrode that is concentric to an inner injector capillary.[38] Instead of using electrophoretic paint for insulation,[33,34] the microring electrode is encapsulated by a borosilicate glass tubing. Consequently, the electrode can be polished and sample solutions can be front- or back-loaded. These attractive features enabled us to conduct sensitive sample analyses in single droplets of ultrasmall volumes (<100 pL) surrounded by an immiscible liquid.[38] In this work, by beveling such an electrode and connecting its back end to a six-port rotary valve and a precision gas displacement pump, we demonstrate that SECM imaging can be performed in the continuous nanoflow (CNF) mode. The resultant apparatus not only provides controllable and stable flows of fresh solution to the center of the microring electrode (which cannot be achieved with a microinjector in the single injection experiment[33]) but also facilitates uninterrupted introduction of samples or mediator solutions through the rotary valve. The CNF-SECM mode obviates interferences from species in the bulk solution or at other areas of the substrate. Using the HRP-amplified protein detection on a microarray platform as an example, we show that reproducible and sensitive imaging of immobilized proteins can be achieved with better resolution and higher sample throughput.

EXPERIMENTAL SECTION

Chemicals and Materials. Ferrocenemethanol ($FcCH_2OH$), ruthenium hexaammine chloride ($Ru(NH_3)_6Cl_3$), bovine serum albumin (BSA), Tween 20, horseradish peroxidase VI (HRP), HRP-labeled antihuman IgG antibody, human IgG, and human IgM were obtained from Sigma-Aldrich (St. Louis, MO). Hydrogen peroxide (H_2O_2; 30%) was acquired from Fisher Scientific (Pittsburgh, PA). Aldehyde-modified glass slides were purchased from Arrayit Corp. (Sunnyvale, CA).

Instrument. Figure 1 shows a schematic diagram of the CNF-SECM instrument. The CNF-SECM probe, mounted

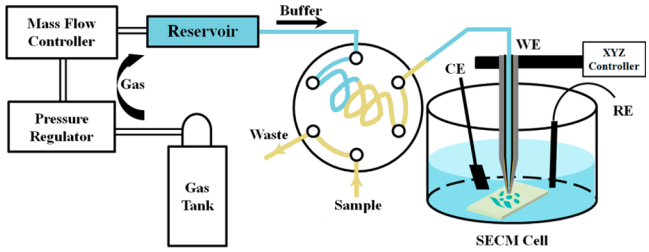

Figure 1. Schematic of the CNF−SECM apparatus. The configuration is for flow of the solution prefilled in the loop (colored in yellow) into the buffer (colored in light blue) through the probe.

onto the stage of an SECM instrument (CHI 900B, Austin, TX), was connected to a six-port rotary valve (Valco Inc., Houston, TX) with tubing sleeves and fingertight PEEK fittings (Upchurch Scientific, Oak Harbor, WA). A home-built gas displacement pump (GDP), consisting of a precision pressure regulator (PRG 101, Omega Engineering, Stamford, CT) and a mass flow controller (model 247D, MKS Instruments, Andover, MA), was used to drive a buffer solution in the reservoir to the injector. The flow rate of the buffer (or carrier solution) is proportional to the volume of gas (N_2) through the mass flow controller and can therefore be calibrated. The lowest flow rate achievable is 1 nL/min, which is 60-fold slower than that attained with a microinjector.[33] Species to initiate surface reactions or to enhance SECM imaging can be introduced to the solution by switching the six-port rotary valve from the "fill" to "deliver" positions. It is worth mentioning that continuous nanoflow can be attained for hours with the 2 μL sample loop. A slow flow rate provides more time for species in the solution to react with molecules confined to the surface. A Pt wire and a saturated Ag/AgCl electrode served as the auxiliary and reference electrodes of the SECM cell, respectively.

Procedure. *Probe Preparation.* The microconcentric ring electrode/injector assembly contains a thin Au film sandwiched between a pulled fused-silica capillary and a borosilicate glass tubing and is constructed as previously described.[38] The CNF-SECM probe was fabricated by beveling its apex on a microcapillary beveler (model BV-10, Buehler, Lake Bluff, IL). During beveling, pressurized air was applied from the back

DOI: 10.1021/acs.analchem.5b00625
Anal. Chem. 2015, 87, 4523−4529

of the capillary to prevent clogging of the injector by polishing materials or broken glass pieces.

Microarray Fabrication. Primary amine groups (NH_2) on HRP, IgG, and IgM can form covalent bonds with the aldehyde groups on the glass slides. To produce microarrays, the glass slides were mounted onto the stage of a microspotter[39] (Wasatch Microfluidics, Salt Lake City, UT). After the printhead was degassed under vacuum to remove bubbles in the microfluidic channels, various concentrations of proteins or 5 mg/mL HRP were allowed to flow through the channel to react with the aldehyde groups for 1 h. Glass slides printed with IgG and IgM were immersed in 1% BSA/phosphate buffer solution (50 mM, pH = 7.4) at room temperature to deactivate the unreacted aldehyde groups. They were then soaked in a phosphate buffer containing 20 μg/mL HRP-labeled anti-IgG/0.5% BSA/0.1% Tween 20 for 1 h. The slides were washed with phosphate buffer thoroughly in between. The PDMS printhead on the microspotter is capable of producing up to 48 oval-shaped spots (~550 μm in the long axis) in a single printing.

CNF-SECM. Before each experiment, the capillary of the probe and the entire flow system was filled by the GDP pump with an electrolyte solution from the reservoir (a large Teflon tubing with an internal volume of ~50 mL). An inert mediator, which is a redox species that does not interfere with the reaction of interest or the imaging process, was dissolved in the electrolyte solution used to fill the SECM cell. For the HRP-catalyzed reaction (cf. eqs 1−3), 1 mM $Ru(NH_3)_6^{3+}$ in a phosphate buffer served as the inert mediator. The GDP pump was turned off while the probe was immersed into the SECM cell. The probe was then positioned at a desired distance above the substrate using the SECM feedback current of $Ru(NH_3)_6^{3+}$. The GDP was turned back on to deliver the buffer solution in the reservoir to the SECM cell at a slow rate (e.g., 15 nL/min). Species used to initiate surface reactions or to enhance SECM imaging were prefilled into and delivered from the 2 μL sample loop mounted on the six-port rotary valve.

RESULTS AND DISCUSSION

Figure 2 illustrates the principle behind CNF-SECM detections of species produced by the nanoflow-initiated and enzyme-catalyzed reactions. Unlike in the conventional SECM generation/collection mode where species diffuse into the tip/substrate gap from the bulk solution, the enzyme substrate/mediator are delivered through the capillary in the middle of the probe and flow radially out of the gap. Specifically, because the small amounts of unreacted H_2O_2 and $FcCH_2OH$ are swept out of the gap and quickly diluted by the buffer solution in the SECM cell, the enzymatic reaction does not proceed at a noticeable extent at other HRP-covered areas of the same surface.

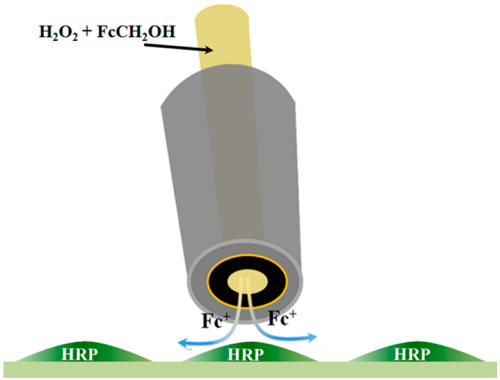

Figure 2. Schematic illustration of the principle of CNF-SECM imaging of enzyme spots (horseradish peroxidase as an example) or spots tagged with enzyme molecules. The flow of ferrocenemethanol and H_2O_2 from the CNF-SECM probe initiates the enzymatic reaction to generate ferriceniummethanol (Fc^+), which is subsequently detected at the microring electrode.

The SEM image in Figure 3A shows a beveled CNF-SECM probe. The inner and outer radii of the microring electrode are 10.9 and 11.5 μm, respectively (inset). Notice that the microring is concentric to the injector whose radius is 5.5 μm. The RG (glass radius/ring radius) value[40] is estimated to be about 5. Because the microring is encapsulated by a borosilicate tubing, our CNF-SECM probe can be beveled and its end be repeatedly polished. Such robustness greatly facilitates the CNF-SECM imaging of large and rough surfaces in the constant-height imaging. The steady-state current of the voltammogram in Figure 3B, 1.73 nA, is in excellent agreement with the theoretical predication.[41] Experimental approach curves over conductive and insulating substrates are presented in Figure 3C, together with the theoretical values deduced using empirical equations[42] with the above-mentioned inner and outer radii and RG number (solid circles). The x-axis is the ratio of the probe/substrate separation, d, over the outer radius of the microring electrode, a. Interestingly, when a redox mediator is introduced through the capillary injector to the middle of the probe/substrate gap, the probe currents over a conducting substrate (cf. dashed red and blue curves in Figure 3C) are substantially smaller than the positive feedback current (upper black curve). Furthermore, the probe current actually increases slightly at $d/a \leq 0.5$ over an insulating substrate (solid red and blue curves), contrary to the negative SECM feedback over an insulator due to hindered diffusion.[2] These results suggest that both redox cycling (over a conductor) and the hindered diffusion (over an insulator) are largely diminished when fresh mediator solution flows radially from the center of the probe out of the probe/substrate gap. Thus, the feedback mode relying on the CNF-delivered mediator is insensitive to both morphological and conductivity changes at a surface. Although the current at the microring electrode can be increased even beyond the positive feedback current at a rather high flow rate (e.g., 1 mL/min used by Macpherson and Unwin[35]), little time would be available for the hydrodynamically delivered species to react with the surface of interest. Moreover, at a high flow rate, the solution composition in the SECM cell will be changed in a short time frame, triggering potentially wanted reactions and increasing the background signal.

The unique advantages of the CNF-SECM mode become apparent when it is used to capture species generated at the surface. To demonstrate this, we first compared the CNF-SECM mode to the conventional SG/TC mode. Figure 4A is the image of a 250 μm-diameter Pt disk substrate obtained by delivering the redox mediator $FcCH_2OH$ through the injector of the probe to the SECM cell. The image shows two advantages over that recorded in the SG/TC mode (Figure 4B). First, the CNF-SECM mode has a higher lateral resolution, as the diameter of the Pt substrate (width at the half height = 262 ± 2 μm) is much closer to the true value than that measured with the conventional G/C mode (318 ± 30 μm). As shown in Figure 4C, the cross-sectional contour attained in the CNF-SECM mode is much less subject to the

DOI: 10.1021/acs.analchem.5b00625
Anal. Chem. 2015, 87, 4523−4529

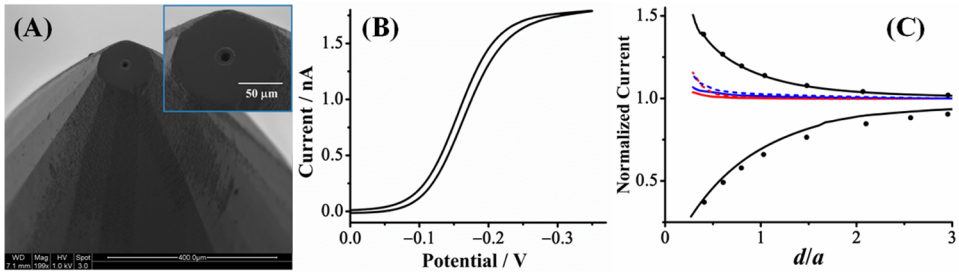

Figure 3. (A) SEM image of a beveled probe. The inset shows the microring (11.5 μm in radius) and capillary injector (5.5 μm). (B) Cyclic voltammogram of 1 mM $Ru(NH_3)_6^{3+}$ in 0.1 M KCl at the microring electrode on the probe. The scan rate was 20 mV/s. (C) Positive (upper black curve) and negative (lower curve) feedback approach curves obtained with the CNF-SECM probe, together with the theoretical fits (black dots) for a 11.5 μm-radius microring. Red and blue curves were obtained by approaching a glass slide (solid) and a thin gold film (dashed) while flowing 1 mM $Ru(NH_3)_6^{3+}$ at 5 and 80 nL/min, respectively. The probe potential was held at −0.4 V vs Ag/AgCl.

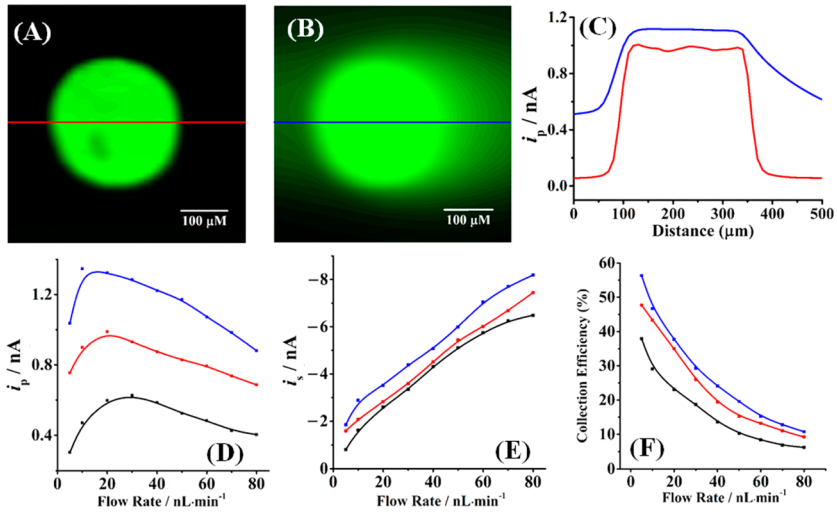

Figure 4. A 250 μm-diameter Pt disk imaged in the CNF-SECM (A) and conventional G/C modes (B) at 50 μm/s using the probe described in Figure 3A. The probe was moved from left to right first. For (A), 1 mM $FcCH_2OH$ was delivered at 20 nL/min, while for (B), a quiescent phosphate buffer containing 1 mM $FcCH_2OH$ was used. In both experiments, d = 11.6 μm and the probe and substrate were kept at 0.0 and 0.5 V vs Ag/AgCl, respectively. (C) Overlays the cross-sectional contours of the Pt disk substrate measured in both modes. Flow rate dependences of the CNF-SECM probe current (i_p in (D)) and the Pt disk substrate (i_s in (E)) at d = 19.0 (black curve), 11.6 (red), and 6.3 μm (blue). The collection efficiencies are shown in (F).

broadening effect associated with the evolving diffusion field encountered in the conventional G/C mode. This is because solution in the probe/substrate gap is constantly and rapidly replenished by fresh solution from the injector of the probe. In fact, we should point out that the lateral resolution of the CNF-SECM mode is governed by the diameter of the injector, which is smaller than that of the microring electrode. We should also add that much smaller capillary injectors can be fabricated with the micropipette puller.[43] However, an extremely small capillary (diameter of ca. 1−2 μm) will be more prone to clogging by colloidal particles in solution and therefore require a particle-free solution and environment for the experiment.[33] Second, in the conventional G/C mode, at a relatively high raster rate, the diffusion field can be disturbed by the moving probe in the rastering direction (cf. Figure 4B). Such a disturbance is absent in the CNF-SECM mode, again due to the much higher flux of surface-generated species transferred by the radial flow than that by diffusion. Although the disturbance in the generation/collection mode can be alleviated by using a slower raster rate, it would take a longer time to complete the imaging of a large surface area and the diffusion field will be even greater on a longer time scale.[2] Sample throughput is particularly important when it comes to microarray imaging.

By positioning the probe over the center of the Pt substrate at various probe/substrate separations, we simultaneously measured the probe and substrate currents i_p and i_s at flow rates ranging from 5 to 80 nL/min. As shown in Figure 4E, an increase in the flow rate leads to a larger flux of $FcCH_2OH$ to the Pt disk and, hence, an augment in i_s.[44] As d decreases, the mediator solution is forced to flow onto the Pt disk at a greater velocity, also resulting in a higher i_s. Interestingly, i_p initially increases with the flow rate but decreases after a maximum. At the optimal flow rate and d, the collection efficiency approaches 60%, a value more than an order of magnitude higher than those relying on only diffusion over the conducting surface.[33,45,46] We should mention that, in the conventional SECM G/C mode, the feedback process interferes with the interpretation of the collection efficiency data. With the flow, the feedback process is essentially eliminated. The maximum shifts to a higher flow rate at larger d. These observations can be rationalized as follows. Mass transfer is contributed by mainly the radial flow at a smaller d and/or a faster flow rate. At a high flow rate, although a greater number of $FcCH_2OH^+$ ions are generated by the Pt substrate, most of them will be rapidly swept out of the probe/substrate gap before being detected by the probe. Consequently, a much increased flow rate will lower

DOI: 10.1021/acs.analchem.5b00625
Anal. Chem. 2015, 87, 4523−4529

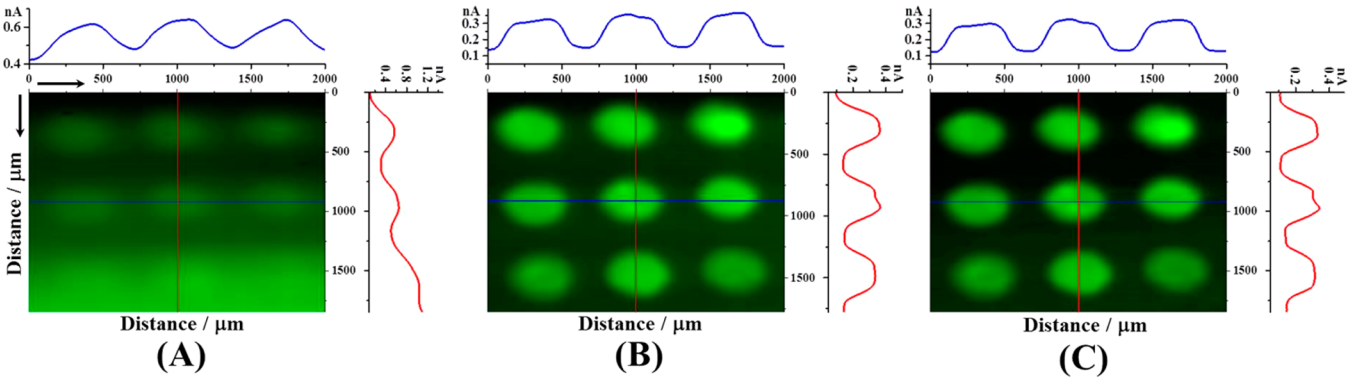

Figure 5. An SECM image of a portion of an 8 × 12 microarray of HRP-covered spots collected by keeping 0.0 V at the CNF-SECM probe in a quiescent solution containing 1 mM $FcCH_2OH$ and 1 mM H_2O_2 (A). The same region was mapped by two consecutive imaging experiments with continuous flow of 1 mM $FcCH_2OH$ and 1 mM H_2O_2 at 15 nL/min into 250 μL of phosphate buffer (B and C). All images were collected at 50 μm/s along the x-direction at d = 11.6 μm. The top and right cross-sectional contours correspond to the spots intersecting with the blue and red lines, respectively. The arrows next to (A) indicate the SECM rastering directions.

the collection efficiency (cf. Figure 4F). This behavior is different from that of a rotating ring/disk electrode at which an increase in rotation or convection increases the amount of products collected by the ring electrode.[7]

As mentioned in the introduction, a problem inherent in using the conventional SECM SG/TC mode for enzyme-amplified microarray imaging is the increasing background current resulted from the steady buildup of the reaction products. This problem is apparent in Figure 5A, which shows a portion of an 8 × 12 array imaged in the conventional SG/TC mode. Even at a relatively fast raster rate (50 μm/s), the spots are somewhat blurry, suggesting that $FcCH_2OH^+$ ions begin to accumulate at and diffuse from each spot as soon as the microarray is immersed in the SECM solution. Moreover, the resolution of the spots is affected by the $FcCH_2OH^+$ ions concurrently generated at and diffused from adjacent spots. Most seriously, by the time the probe rastered over the third row, the spots had become almost indistinguishable from the background. In fact, when such an array was immersed in a 250 μL solution, the pale yellow $FcCH_2OH$ solution changed into the blue-colored $FcCH_2OH^+$ solution within 1 h. Thus, reproducibility (replicate imaging) and accuracy (i.e., detection of spots of the same or different surface densities) are at issue when high-density arrays are imaged in the conventional G/C mode.

This problem can be circumvented by using the CNF-SECM mode wherein only the spot being imaged is exposed to sufficient amounts of the enzyme substrate and redox mediator. For our probe to collect $FcCH_2OH^+$ generated at the surface, the same dependence on the flow rate as that exhibited in Figure 4D was observed. This suggests that the kinetics of the HRP-catalyzed reaction is as fast as the facile electron transfer reaction of the Fc/Fc^+ couple and the overall enzymatic reaction is mass transfer controlled. At 15 nL/min, images of spots with highly comparable shapes and intensities can be repeatedly collected (Figure 5B,C). Notice that no change in the background of Figure 5B,C is discernible. This is understandable as the solution in the probe/substrate gap is always isolated from the bulk by fresh $FcCH_2OH$ delivered from the CNF system. We should note that the bulk solution composition will not be altered appreciably by continuous flow of species over an extended period of time. For example, a continuous flow of 1 mM H_2O_2 at 15 nL/min for 4 h into 250 μL of phosphate buffer will increase the bulk H_2O_2 concentration to only 0.014 mM. Such a change is even overestimated because a fraction of H_2O_2 has reacted away when the CNF-delivered solution flows over the HRP-covered spots. In any case, the change is too small to induce any unwanted reactions at other sites of the surface. A comparison between Figure 5A,B also reveals that the resolution in the latter is higher, because of the two advantages mentioned above. The long axis of the oval spot (562 ± 8) is quite close to the actual spot size (550 μm for the particular printhead we used).

We then evaluate the performance of the CNF-SECM mode for selective detection of immobilized proteins. Figure 6 is a 2 × 4 array with 0.665 μM human IgG and IgM spotted alternatingly in each row. As can be seen, only the IgG spots are visible, because they specifically interact with HRP-labeled anti-IgG.

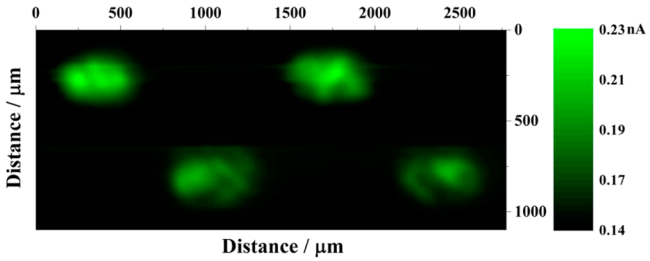

Figure 6. A CNF-SECM image of a 2 × 4 human IgG/IgM microarray. Other experimental conditions are the same as those for Figure 5B.

The final experiment is concerned with the detection level of the CNF-SECM mode. Figure 7 shows an array composed of four rows of IgG spots of different surface densities. The 1.333 μM spots yield the highest current, and the diminishing current intensity is clearly visible over the 1.333 and 0.067 μM spots. The contrast between the 0.067 and 0.013 μM is more obvious from the cross-sectional contour (cf. the red curve on the right). Linear regression of the data yielded i (nA) = 0.23 [IgG] (μM) + 0.10 (R^2 = 0.98). On the basis of 3σ of the background, the detection limit of IgG was determined to be 3.0 nM. Such a value compares favorably to those obtained with the conventional SG/TC mode imaging of enzyme-labeled protein microarrays.[27,47] The attainment of a lower detection limit

DOI: 10.1021/acs.analchem.5b00625
Anal. Chem. 2015, 87, 4523−4529

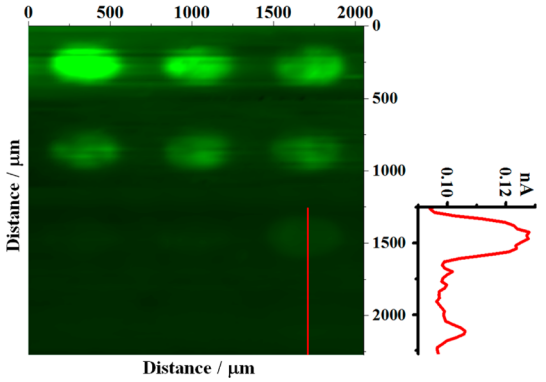

Figure 7. A CNF-SECM image of a microarray spotted with four different concentrations (0.013, 0.067, 0.665, and 1.333 μM) of human IgG solutions (from bottom to top). Other experimental conditions are the same as those in Figure 6.

stems from the aforementioned elimination of background interference. The microspotter we used is for rapid fabrication of large spots of protein microarrays and typically requires ca. 50 μL (or 150 fmol in the present case) of protein solution for each spot. For other types of arrays (e.g., DNA or antibody arrays), smaller spots can be made with other types of microarrayers.[48] With the higher sensitivity and resolution, the CNF-SECM mode can help further reduce the already remarkably low sample consumption.

CONCLUSION

We have systematically characterized the voltammetric behavior of a beveled microconcentric ring electrode/injector as an SECM probe. Owing to the encapsulation of the microring electrode/injector into a borosilicate tubing, the probe is rugged and can be repeatedly polished. By connecting this probe to a continuous nanoflow system, higher resolution than that obtainable with the conventional SECM generation/collection mode can be achieved. Moreover, the CNF-SECM imaging is versatile as different reactants or species can be introduced through the injector to the probe/substrate gap to initiate surface reactions. Because solutions can be delivered at a rather slow flow rate (e.g., 1 nL/min), little change occurs in the bulk SECM solution, reducing the background current and avoiding artifacts that might be encountered in the conventional generation/collection mode. The CNF-SECM mode was used to obtain highly reproducible and accurate HRP-amplified images of protein microarrays, which can be readily extended to imaging of samples labeled with other types of enzymes. Although not investigated in this study, we believe that the CNF-SECM mode should be attractive for imaging in complex sample media wherein various species that could potentially "foul" a regular SECM probe are isolated from the media by the CNF-delivered solution used for imaging.

AUTHOR INFORMATION

Corresponding Author

*E-mail: fzhou@calstatela.edu.

Notes

The authors declare no competing financial interest.

ACKNOWLEDGMENTS

Partial support of this work by a National Science Foundation grant (NSF 1112105), the National Key Basic Research Program of China (2014CB744502), and the NSF-CREST Program at California State University, Los Angeles (NSF HRD-0931421), is gratefully acknowledged.

REFERENCES

(1) Bard, A. J.; Fan, F. F.-R.; Pierce, D. T.; Unwin, P. R.; Wipe, D. O.; Zhou, F. *Science* **1991**, *254*, 68−74.
(2) Bard, A. J., Mirkin, M. V., Eds. *Scanning Electrochemical Microscopy*, 2nd ed.; CRC Press: Boca Raton, FL, 2012.
(3) Schulte, A.; Schuhmann, W. *Angew. Chem., Int. Ed.* **2007**, *46*, 8760−8777.
(4) Sun, P.; Laforge, F. O.; Mirkin, M. V. *Phys. Chem. Chem. Phys.* **2007**, *9*, 802−823.
(5) Amemiya, S.; Bard, A. J.; Fan, F. R. F.; Mirkin, M. V.; Unwin, P. R. *Annu. Rev. Anal. Chem.* **2008**, *1*, 95−131.
(6) Schulte, A.; Nebel, M.; Schuhmann, W. *Annu. Rev. Anal. Chem.* **2010**, *3*, 299−318.
(7) Bard, A. J.; Faulkner, L. R. *Electrochemical Methods: Fundamentals and Applications*; John Wiley & Sons: New York, 2001.
(8) Skoog, D.; Holler, F.; Crouch, S. *Principles of Instrumental Analysis*, 6th ed.; Thomson Higher Education: Belmont, CA, 2007.
(9) Zhou, F.; Unwin, P. R.; Bard, A. J. *J. Phys. Chem.* **1992**, *96*, 4917−4924.
(10) Wittstock, G.; Yu, K. J.; Halsall, H. B.; Ridgway, T. H.; Heineman, W. R. *Anal. Chem.* **1995**, *67*, 3578−3582.
(11) Wang, J.; Song, F. Y.; Zhou, F. *Langmuir* **2002**, *18*, 6653−6658.
(12) Turcu, F.; Schulte, A.; Hartwich, G.; Schuhmann, W. *Angew. Chem., Int. Ed.* **2004**, *43*, 3482−3485.
(13) Diakowski, P. M.; Kraatz, H. B. *Chem. Commun.* **2009**, 1189−1191.
(14) Wain, A. J.; Zhou, F. *Langmuir* **2008**, *24*, 5155−5160.
(15) Fernandez, J. L.; Walsh, D. A.; Bard, A. J. *J. Am. Chem. Soc.* **2005**, *127*, 357−365.
(16) Bhattacharya, C.; Lee, H. C.; Bard, A. J. *J. Phys. Chem. C* **2013**, *117*, 9633−9640.
(17) Liu, B.; Rotenberg, S. A.; Mirkin, M. V. *Proc. Natl. Acad. Sci. U. S. A.* **2000**, *97*, 9855−9860.
(18) Kurulugama, R. T.; Wipf, D. O.; Takacs, S. A.; Pongmayteegul, S.; Garris, P. A.; Baur, J. E. *Anal. Chem.* **2005**, *77*, 1111−1117.
(19) Koley, D.; Bard, A. J. *Proc. Natl. Acad. Sci. U. S. A.* **2010**, *107*, 16783−16787.
(20) Takahashi, Y.; Shevchuk, A. I.; Novak, P.; Babakinejad, B.; Macpherson, J.; Unwin, P. R.; Shiku, H.; Gorelik, J.; Klenerman, D.; Korchev, Y. E.; Matsue, T. *Proc. Natl. Acad. Sci. U. S. A.* **2012**, *109*, 11540−11545.
(21) Nebel, M.; Grutzke, S.; Diab, N.; Schulte, A.; Schuhmann, W. *Angew. Chem., Int. Ed.* **2013**, *52*, 6335−6338.
(22) Basame, S. B.; White, H. S. *Anal. Chem.* **1999**, *71*, 3166−3170.
(23) Alpuche-Aviles, M. A.; Baur, J. E.; Wipf, D. O. *Anal. Chem.* **2008**, *80*, 3612−3621.
(24) Wilson, D. S.; Nock, S. *Angew. Chem., Int. Ed.* **2003**, *42*, 494−500.
(25) Wittstock, G.; Burchardt, M.; Pust, S. E.; Shen, Y.; Zhao, C. *Angew. Chem., Int. Ed.* **2007**, *46*, 1584−1617.
(26) Wain, A. J. *Electrochem. Commun.* **2014**, *46*, 9−12.
(27) Shiku, H.; Matsue, T.; Uchida, I. *Anal. Chem.* **1996**, *68*, 1276−1278.
(28) Ciobanu, M.; Taylor, D. E.; Wilburn, J. P.; Cliffel, D. E. *Anal. Chem.* **2008**, *80*, 2717−2727.
(29) Neugebauer, S.; Zimdars, A.; Liepold, P.; Gebala, M.; Schuhmann, W.; Hartwich, G. *ChemBioChem* **2009**, *10*, 1193−1199.
(30) Takahashi, Y.; Miyamoto, T.; Shiku, H.; Asano, R.; Yasukawa, T.; Kumagai, I.; Matsue, T. *Anal. Chem.* **2009**, *81*, 2785−2790.
(31) Momotenko, D.; Qiao, L.; Cortes-Salazar, F.; Lesch, A.; Wittstock, G.; Girault, H. H. *Anal. Chem.* **2012**, *84*, 6630−6637.
(32) Palatzky, P.; Matysik, F. M. *Electroanalysis* **2011**, *23*, 50−54.
(33) Walsh, D. A.; Fernández, J. L.; Mauzeroll, J.; Bard, A. J. *Anal. Chem.* **2005**, *77*, 5182−5188.

DOI: 10.1021/acs.analchem.5b00625
Anal. Chem. 2015, 87, 4523−4529

(34) Xiong, H.; Guo, J. D.; Kurihara, K.; Amemiya, S. *Electrochem. Commun.* **2004**, *6*, 615−620.
(35) Macpherson, J. V.; Unwin, P. R. *Anal. Chem.* **1998**, *70*, 2914−2921.
(36) Macpherson, J. V.; Jones, C. E.; Unwin, P. R. *J. Phys. Chem. B* **1998**, *102*, 9891−9897.
(37) Macpherson, J. V.; Unwin, P. R. *Anal. Chem.* **1999**, *71*, 2939−2944.
(38) Kai, T. H.; Chen, S.; Monterroso, E.; Hailu, A.; Zhou, F. *Anal. Chem.* **2014**, *86*, 8037−8041.
(39) Eddings, M. A.; Miles, A. R.; Eckman, J. W.; Kim, J.; Rich, R. L.; Gale, B. K.; Myszka, D. G. *Anal. Biochem.* **2008**, *382*, 55−59.
(40) Bard, A. J.; Fan, F. R. F.; Kwak, J.; Lev, O. *Anal. Chem.* **1989**, *61*, 132−138.
(41) Lee, Y.; Amemiya, S.; Bard, A. J. *Anal. Chem.* **2001**, *73*, 2261−2267.
(42) Cornut, R.; Mayoral, M.; Fabre, D.; Mauzeroll, J. *J. Electrochem. Soc.* **2010**, *157*, F77−F82.
(43) Brown, K. T.; Flaming, D. G. *Advanced Micropipette Techniques for Cell Physiology*; Wiley and Sons: New York, 1986.
(44) Macpherson, J. V.; Marcar, S.; Unwin, P. R. *Anal. Chem.* **1994**, *66*, 2175−2179.
(45) Liljeroth, P.; Johans, C.; Slevin, C. J.; Quinn, B. M.; Kontturi, K. *Anal. Chem.* **2002**, *74*, 1972−1978.
(46) Liljeroth, P.; Johans, C.; Slevin, C. J.; Quinn, B. M.; Kontturi, K. *Electrochem. Commun.* **2002**, *4*, 67−71.
(47) Shiku, H.; Hara, Y.; Matsue, T.; Uchida, I.; Yamauchi, T. *J. Electroanal. Chem.* **1997**, *438*, 187−190.
(48) Barbulovic-Nad, I.; Lucente, M.; Sun, Y.; Zhang, M. J.; Wheeler, A. R.; Bussmann, M. *Crit. Rev. Biotechnol.* **2006**, *26*, 237−259.

DOI: 10.1021/acs.analchem.5b00625
Anal. Chem. 2015, 87, 4523−4529